

Extended Hückel theory for bandstructure, chemistry and transport.

I. Carbon Nanotubes

D. Kienle,^{1,*} J.I. Cerda,² and A.W. Ghosh³

¹*Purdue University, Department of Electrical and Computer Engineering, West Lafayette, IN 47907, USA*

²*Instituto de Ciencia de Materiales de Madrid, CSIC, Cantoblanco 28049, Madrid, Spain*

³*University of Virginia, Department of Electrical and Computer Engineering, Charlottesville, VA 22903, USA*

(Dated: February 5, 2008)

We describe a semi-empirical atomic basis Extended Hückel Theoretical (EHT) technique that can be used to calculate bulk bandstructure, surface density of states, electronic transmission and interfacial chemistry of various materials within the same computational platform. We apply this method to study multiple technologically important systems, starting with carbon-nanotubes (CNT) and their interfaces in this paper, and silicon-based heterostructures in our follow-up paper. We find that when it comes to quantum transport through interesting, complex heterostructures, the Hückel bandstructure offers a fair and practical compromise between orthogonal tight-binding theories (OTB) with limited transferability between environments under large distortion, and density functional theories (DFT) that are computationally quite expensive for the same purpose.

PACS numbers: 61.46.Fg, 73.43.Cd, 73.63.Fg

I. INTRODUCTION

Quantitative electronic structure theories are essential to the understanding and designing of novel materials and devices. It is now generally accepted that transport properties of nanoscale devices depend on both the intrinsic electronic structure of the active channel, as well as its interfacial properties with contacts and other scattering centers. A particular challenge in this respect is to incorporate both long and short range correlations within the same framework, such as the bulk bandstructure of periodic solids as well as the local chemical properties of clusters, surfaces, and interfaces. For instance, simulating scanning tunneling spectra (STS) of molecules on silicon substrates requires an accurate description of the silicon bulk bandstructure that quantitatively captures not just the bandgap responsible for the onset of negative differential resistance,¹ but also the multiple effective masses which determine the contact density of states and injection velocities, and the strain parametrizations that capture atomic reconstruction and relaxation near the surface and their bonding with molecular components.² In addition, one needs to describe the electrostatics responsible for band-bending in the silicon depletion layer, the molecular transport levels and their transmission under bias, and finally the electronic properties of the scanning tip and the intervening vacuum layer, all within the same formalism. It is no surprise therefore that under these circumstances, standard electronic structure techniques developed by quantum chemists for simulating molecules are usually incompatible with those developed by solid-state physicists for bulk bandstructure, making it important to develop a common formalism that addresses both domains of interest and also maintains a good compromise between computational accuracy and practicality.

While sophisticated methods exist for equilibrium ge-

ometry and bandstructure, comparable success has yet to be achieved for transport problems, partly because of the lack of universally accepted experimental standards, but mainly because quantum transport inherently involves solving a complicated nonequilibrium open boundary problem for which electronic structure theories are not benchmarked. A proper quantitative understanding of correlation effects in transport is still evolving and it is not yet clear if mean-field approaches that work at equilibrium are at all capable of handling the profusion of electronic excitations that often dominate in nanoscale conduction.^{3,4} Even aside from such correlation issues, one needs to worry about heterointerfaces since current flow involves charge transport across two intrinsically different material systems – a multimoded contact consisting of a highly conductive material externally maintained at thermal equilibrium, and a sparsely moded device region that is readily driven away from equilibrium and acts as the active transport channel.

In this paper, we employ a semi-empirical approach to electronic structure that can be adopted for electronic conduction through complex hybrid systems by combining it with the Nonequilibrium Green's function (NEGF) technique for quantum transport. Our theoretical parameters are tailored to salient features of the bulk bandstructure, while the employment of non-orthogonal basis sets resembling linear combinations of underlying atomic orbitals seems to make them fairly transferrable to surfaces as well, as observed in the past.^{5,6} In addition, the presence of explicit basis sets opens up the possibility of 'stitching' together disparate regions⁷ by matching the interfacial Green's function, which is the *only* quantity through which the diverse regions communicate with each other quantum mechanically. The modularity of our approach also allows us to conveniently separate the problems of determining the optimized interfacial geometry and the interfacial transmission (we are ignoring current-induced forces), the former depending on the to-

tal energy of the system while the latter depends only on a few relevant single-electron levels near the Fermi energy. In other words, *given a particular atomistic configuration of the contact-channel-contact heterostructure, we seek to determine its transport properties by coupling our electronic structure approach with quantum transport using NEGF.*

The outline of the paper is as follows: section II explains the strengths of EHT over other traditional bandstructure methods. In section III we briefly summarize the NEGF approach used to calculate density of states and transmission of CNTs; we then specify the model Hamiltonian and describe the details of EHT used to determine the bandstructure. The numerically calculated bandstructure data for nanotubes are then compared in section IV with experimental scanning tunneling spectroscopy experiments along with other theoretical approaches. In section V we investigate the changes in the dispersion of a semi-conducting CNT under large lateral deformations as well as with a CO molecular attachment to its surface that allows it to function as a molecular sensor. We summarize our work and discuss future extensions in the last section.

II. WHY THIS PARTICULAR METHOD?

A particular trade-off in any bandstructure theory is between flexibility and rigor. While empirical, orthogonal tight-binding (OTB) methods are quick and practical, they are benchmarked for specific geometries and are usually not very transferable to other environments involving significant structural deformations beyond a few percent. Tight binding basis-sets are commonly assumed to be both orthogonal and short-ranged,⁵ while atomic wavefunctions are not, meaning that OTB basis sets do not resemble eigenstates of an atomic Hamiltonian. Efforts at improving tight-binding theories involve going beyond nearest neighbor techniques, using higher virtual orbital bases for increased completeness,^{8,9,10} and employing power laws for parameter transfer under small ($\sim 1 - 2\%$) strain.¹¹ Nevertheless these models are likely to miss important chemical details involving properties varying on an interatomic length scale, in particular near deformed surfaces and interfaces where a drastic reconstruction of the atomic structure is expected.⁵

At the other end of the spectrum are accurate, but computationally expensive first-principles techniques developed by quantum chemists and solid state physicists, such as Configuration Interaction (CI) and Density Functional Theories (DFT) in various atomic or plane wave basis sets or combinations thereof. Structural deformations are naturally captured by such total energy calculations by solving a one electron Schrödinger equation in a suitable self-consistent potential approximating the electron-electron interaction.^{12,13,14} Such codes are typically based on rigorous variational theorems and are quantitatively quite accurate, at least for equilib-

rium properties. Their extension and practical implementation to transport beyond the linear response regime is continuously evolving,^{15,16,17} and a topic of current research.¹⁸ Conceptually, it is not clear if any self-consistent potential approach can quantitatively describe the rich spectrum of many-body transitions that are often experimentally accessed in strongly correlated transport in weakly coupled systems.^{3,4}

We aim for a practical compromise between these two limits by using a semi-empirical technique motivated by Extended-Hückel calculations popular in the chemistry community. Such theories, widely used in the past to describe the equilibrium properties of isolated molecules,¹⁹ have recently been applied to molecular conduction²⁰ and also extended to solids using transferable atomic-orbital basis sets (AO) for calculating the electronic structure of various compounds benchmarked with detailed DFT calculations within the local density (LDA) or generalized gradient (GGA) approximations.²¹ Given a geometry, one uses the explicit EHT basis functions to calculate a non-orthogonal overlap matrix S , which along with separately fitted onsite Hamiltonian matrix elements yields the corresponding off-diagonal hopping elements of the Hamiltonian. Within the standard Hückel prescription, structural changes are simply accounted for by re-calculating the overlap and hopping elements, but leaving the basis sets and onsite elements unchanged.

In the following, we apply this EHT parametrization scheme²¹ by benchmarking it to a two-dimensional graphene sheet^{22,23} and extending it to obtain the bandstructure, density of states and electronic transmission of carbon nanotubes (CNT) of varying chiralities. We show that the same bulk-optimized EHT-parameters (onsite energies and AO-basis functions) are transferable to small diameter CNT bandstructures, capturing even curvature-induced bandgap effects for larger than $1 - 3\%$ tube deformation, in quantitative agreement with STS data. Furthermore, surface chemical effects are examined through the study of nanotube based carbon-monoxide sensors whose alteration of electronic structure upon molecular adsorption compares favorably with ab-initio calculations of da Silva *et al.*²⁴ In our follow-up paper, we will demonstrate a similar transferability between bulk silicon, various silicon surfaces, apply the EHT-methodology to unreconstructed silicon nanowires. Taken together, the wide variety of these examples illustrates the range of transferability of EHT parameters, which we believe makes Extended Hückel Theory a useful practical tool for electronic structure and quantum transport.

III. APPROACH

Simulating conduction through a heterostructure involves combining suitable bandstructures for the channel and contact materials with self-consistent electrostatics and quantum transport. While the formulation of cor-

related transport is itself an active area of research, our aim here is to develop a minimal model that would capture quantum chemistry, surface physics, bandstructure and electrostatic effects that are all crucial for different prominent aspects of nanoscale conduction. The ingredients needed for a proper simulation are the Hamiltonian and potential matrices describing the device bandstructure and electrostatics, and the contact self-energies that effectively open up the system and allow us to add or remove charge under nonequilibrium conditions. The EHT prescription gives us a practical way to calculate these ingredient matrices for a given atomistic structure, and then connect them with a non-equilibrium Green's function (NEGF) formulation of quantum transport, which we briefly summarize below.^{25,26} The retarded Green function of the device is given by

$$G = [(E + i\eta)S - H - \Sigma_l - \Sigma_r]^{-1} , \quad (1)$$

where S and H describe the overlap and Hamiltonian matrices of the device unit cell calculated according to the Hückel prescription Eq.(5). The matrix elements $\Sigma_{l,r}$ are self-energies that provide open boundary conditions to the device with the left and right semi-infinite contacts. The self-energy $\Sigma = \tau g \tau^\dagger$ incorporates the coupling matrix τ describing the contact-device bonding, while g is the surface Green function of the left/right contact calculated by means of a recursion technique.^{27,28} In a non-orthogonal tight-binding scheme the density of states (DOS) is given by $D(E) = \frac{i}{2\pi} \text{Tr}(AS)$ where $A = i(G - G^\dagger)$ denotes the spectral function. Finally, in the phase-coherent limit the zero-bias transmission through the unit cell reads $T(E) = \text{Tr}[\Gamma_l G \Gamma_r G^\dagger]$, where $\Gamma_{l,r} = i(\Sigma_{l,r} - \Sigma_{l,r}^\dagger)$ are the broadening matrices which specify the time an electron resides within the device. In this paper, we will study infinite nanotubes so that the active device is just one CNT unit cell and the left and right contacts extend that cell to infinity in either direction.

The bandstructure of a nanotube with chirality (n, m) is calculated employing the non-orthogonal Slater-Koster scheme and solving for the generalized eigenvalue problem²⁹

$$\mathbf{H}(\mathbf{k})A_i(\mathbf{k}) = E_i(\mathbf{k})\mathbf{S}(\mathbf{k})A_i(\mathbf{k}) , \quad (2)$$

where $A_i(\mathbf{k})$ denotes the eigenvector of the i^{th} subband, and \mathbf{k} is a Bloch wavevector within the first Brillouin zone. The size of the overlap and Hamiltonian matrices are determined by the chosen basis set, i.e., the number of atoms within the unit cell multiplied by the number of orbitals per atom. In our case, using four sp -orbitals per atom, the size of these matrices is 80×80 for an armchair (5, 5) tube as sketched in Fig. 1. The overlap and Hamilton matrices $\mathbf{S}(\mathbf{k})$ and $\mathbf{H}(\mathbf{k})$ representing the structure in reciprocal space are calculated by

$$\mathbf{H}_{i,j}(\mathbf{k}) = \sum_{j',m'} e^{i\mathbf{k} \cdot (\mathbf{R}_{i0} - \mathbf{R}_{j'm'})} \mathbf{H}_{i0,j'm'} \quad (3)$$

$$\mathbf{S}_{i,j}(\mathbf{k}) = \sum_{j',m'} e^{i\mathbf{k} \cdot (\mathbf{R}_{i0} - \mathbf{R}_{j'm'})} \mathbf{S}_{i0,j'm'} , \quad (4)$$

where i, j label atoms within the unit cell, and m' is the unit cell index. The summation indices in $\mathbf{H}_{i,j}(\mathbf{k})$, $\mathbf{S}_{i,j}(\mathbf{k})$ run over all atoms j' in unit cell m' which are equivalent to atom j in the reference unit cell $m = 0$. The real-space matrix elements $\mathbf{H}_{i0,j'm'}$, $\mathbf{S}_{i0,j'm'}$, between an atom i in the reference unit cell and atom j' in cell m' are calculated by means of the Extended Hückel prescription.

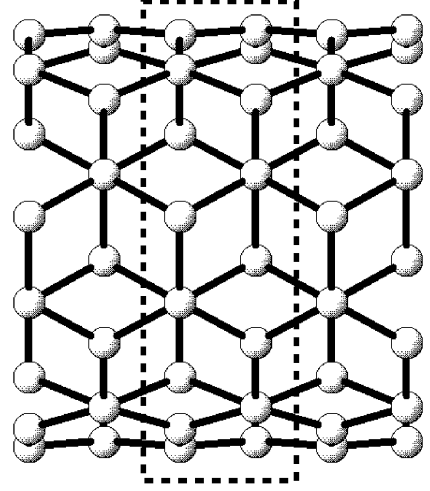


FIG. 1: Sketch of a (5, 5) armchair tube with three unit cells. The dashed rectangle marks the center unit cell containing 20 carbon atoms. For the calculation of the $E - k$ dispersion we use the 1st nearest-neighbor unit cells to the left and right, respectively.

Perhaps the most prominent difference between the empirical tight-binding and EHT principle is the use of an irreducible representation of the tight-binding Hamiltonian which is directly fitted to available bandstructure data without employing explicit basis sets. In EHT however one works directly with the orbital basis functions out of which the Hamiltonian elements are constructed using the Hückel principle. The diagonal elements are benchmarked with experimental values of electronic ‘hardness’, i.e. the difference between ionization potential and electron affinity.¹⁹ The off-diagonal matrix elements are then determined directly from the prescription

$$\begin{aligned} H_{\mu\mu} &= E_{\mu\mu}, \\ H_{\mu\nu} &= \frac{1}{2} K_{eht} S_{\mu\nu} (H_{\mu\mu} + H_{\nu\nu}) , \\ S_{\mu\nu} &= \int d^3\mathbf{r} \phi_\mu^*(\mathbf{r}) \phi_\nu(\mathbf{r}) , \end{aligned} \quad (5)$$

where μ, ν label the atomic orbitals, and $S_{\mu\nu}$ is the overlap matrix between the orbital basis function ϕ_μ and ϕ_ν , respectively. K_{eht} is an additional fitting parameter with a value of 1.75 commonly used for molecules

and 2.3 for solids.^{19,21} In the case of the planar 2D-graphene sheet a good match is achieved for a value of $K_{eht} = 2.8$.²² One important assumption within EHT is that the hopping matrix elements $H_{\mu\nu}$, $\nu \neq \mu$ depend linearly on the overlap matrix $S_{\mu\nu}$ alone.¹⁹ EHT-basis functions are usually Slater-type orbitals (STO), $\Phi_{nlm} = N r^{n-1} e^{-\zeta r} Y_{lm}(\Theta, \varphi)$, which have the correct asymptotic form at large distance r (n , l , and m denote respectively the principle, azimuthal and magnetic quantum numbers). The individual orbital wavefunctions $|q\rangle$ are then approximated by a linear combination of STOs, with coefficients and exponents $\{c_i, \zeta_i\}$ fitted for the individual basis functions to match bandstructure data. Since the basis sets are directly fitted to experimental or theoretical data, the resulting AOs are more localized than the free atomic wavefunctions, although they may still be regarded as long-ranged compared to the usual TB Wannier-like description; we typically use a cut-off interatomic distance of $R_c = 9 \text{ \AA}$ for the interactions. The use of basis function that are not too localized turns out to be a key issue for achieving a good transferability.²¹ Admittedly, the use of a direction independent K_{eht} function is a drastic assumption that can be relaxed by making the constant orbital dependent, but we make the simplifying assumption that the orientation dependence arises principally from the corresponding overlap functionals.

The Hückel prescription Eq. (5) can be generalized to connect different chemical sub-systems A, B . The problem is that each sub-system has its own parametrization that yields its own vacuum level relative to which electronic levels are calculated. For instance, the Fermi level of most metals is set to $E_F = -10 \text{ eV}$ in the paper in,²¹ which means that each dispersion curve needs to be individually shifted to bring its Fermi level up to the experimental value, through the transformation $\mathbf{H} \rightarrow \mathbf{H} + V_c \mathbf{S}$ for each sub-system. The correct alignment of the levels relative to each other becomes particularly important when studying compound systems such as metal-semiconductor junctions or molecular components attached on nanowires and nanotubes. We calculate the coupling matrix across such a hybrid junction between subsystems A and B using the Hückel principle Eq.(5) through the interpolation scheme

$$\tilde{\mathbf{H}}_{\mu A \nu B} = \frac{1}{2} \mathbf{S}_{\mu A \nu B} [(K_A \mathbf{H}_{\mu\mu}^A + V_{cA}) + (K_B \mathbf{H}_{\nu\nu}^B + V_{cB})] , \quad (6)$$

where V_{cA} and V_{cB} are the shifts needed to align the vacuum levels for sub-systems A and B , respectively. It is worth noting that this approach provides a simple interpolation scheme that gives us the correct limiting values of the Hamiltonian for the two individual subsystems. Further work, however, clearly needs to be done to calibrate this interpolation scheme to specific interfacial properties such as measured charge transfer doping, Schottky barrier heights, or perhaps first principles calculations of interfacial dipoles or chemisorption properties

such as workfunction modification at surfaces.

IV. RESULTS: NANOTUBE BANDSTRUCTURES

We begin by benchmarking our parameters with a two-dimensional graphene sheet. Figure 2 shows the corresponding dispersion relation along the $M \rightarrow \Gamma \rightarrow K \rightarrow M$ path within the 2D-Brillouin zone. The dashed line in Fig.2 is the DFT-GGA calculation of the $E-k$ dispersion calculated using the SIESTA code,^{22,23} to which the EHT bandstructure is fitted (solid line) by adjusting the on-site Hamiltonian matrix-elements H_{ii} , the exponentials and the expansion coefficients of the Slater-orbital basis functions. As atomic like basis functions for each carbon atom we are using two basis sets: (i) sp^3 and (ii) sp^3d^5 orbitals, each of which has been optimized to match the DFT-GGA bandstructure. The two parameter sets are given in Table I. In our calculation all atoms within a cut off radius of 9 \AA from the two non-equivalent atoms within a unit cell are included. Furthermore, we set the Fermi level of graphene to $E_F = 0.0 \text{ eV}$ and K_{eht} is set to 2.8.⁵²

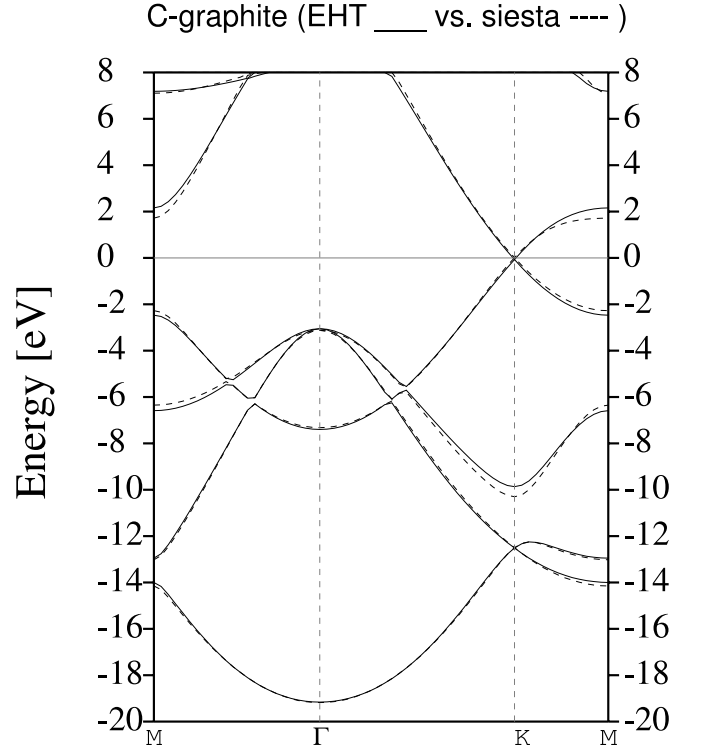


FIG. 2: 2D bandstructure of a graphene sheet along the $M \rightarrow \Gamma \rightarrow K \rightarrow M$ path within the 1st Brillouin zone. The solid line corresponds to the EHT-bandstructure using parameters optimized to match the DFT-GGA bandstructure (dashed line).^{22,23} The C-C bonding distance is set to $a_{C-C} = 1.44 \text{ \AA}$, and the cut-off radius for the neighbor atoms is $R_c = 9 \text{ \AA}$. The Fermi level is at $E_F = 0.0 \text{ eV}$.

	AO	E_{on}	ζ_1	c_1	ζ_2	c_2
C-sp	2s	-20.316	2.037	0.741	3.249	0.412
	2p	-13.670	1.777	0.640		
C-sp ^d	2s	-19.889	2.025	0.764	2.177	0.739
	2p	-13.080	1.624	0.272		
	3d	-2.046	1.194	0.491		

TABLE I: EHT parameters for carbon fitted to the 2D-bandstructure of graphene calculated using DFT-GGA.^{22,23} For both parameter sets the parameter K_{eht} was set to 2.8.

Carbon-nanotubes with chirality (n, m) are obtained by wrapping the two dimensional graphene sheet along specific circumference vectors $\mathbf{C}(n, m) = n\mathbf{a}_1 + m\mathbf{a}_2$.³⁰ Note that this approach, being truly atomistic, goes beyond the conventional zone-folding scheme. In the following, we will examine the transferability of the two EHT parameter sets (sp and spd) of graphene to bandstructures for small diameter nanotubes. In our calculation, we assume that structural variations of the CNT affect its hopping elements H_{ij} only through the overlap matrix S_{ij} (cf. Eq. 5). This assumption means that the re-distribution of charge due to structural changes is discarded, so that the bandstructure is determined in a non self-consistent manner. For all tubes considered here we include the coupling of nearest neighbor unit cells which consist of two rings each in the case of armchair (n, n) tubes (translation vector $T_0 = 2.39 \text{ \AA}$), and four rings for zig-zag $(n, 0)$ CNTs ($T_0 = 4.32 \text{ \AA}$).

A. Metallic armchair tubes

Fig. 3 shows the bandstructure, transmission and density-of-states (DOS) for a (5,5) armchair tube within a sp^3 -EHT model. The DOS shows typical features of a one-dimensional system, with a constant value within an energy interval of $[-1.5, 1.5] \text{ eV}$, and van Hove singularities at the onsets of higher subbands. The transmission per spin within the interval $[-1.5, 1.5] \text{ eV}$ is 2 indicating that two bands can in principle contribute to transport. Including spin, one should then observe a maximum linear response (zero bias) conductance of $G = 2G_0$ with $G_0 = 2e^2/h$ assuming no parasitic resistances posed by contact interfaces. Notably, curvature effects do not disrupt the bandstructure of armchair tubes, which stay metallic because the mirror symmetry is not broken upon wrapping the graphene sheet.

B. Curvature effects on non-armchair ‘semi-metallic’ tubes

Experimentally it is known that small diameter carbon nanotubes that are normally expected to be metallic by the $m - n$ rule,³⁰ with (9,0) and (12,0) chiralities for example, exhibit a curvature-induced gap than

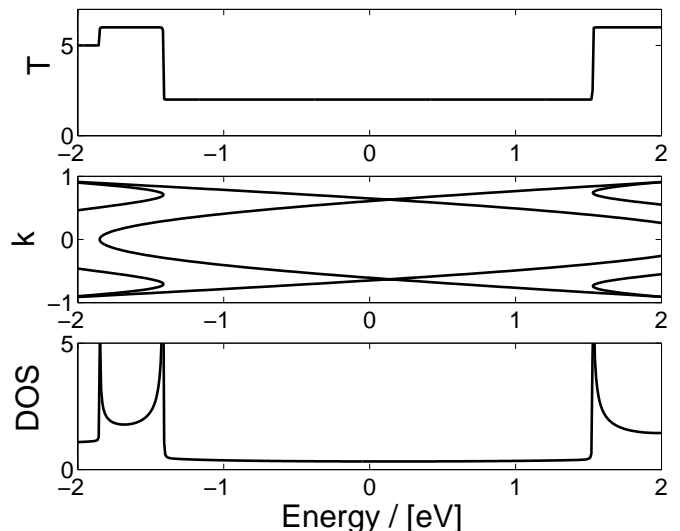


FIG. 3: Bandstructure, transmission and DOS per spin for an armchair (5,5) tube using sp^3 -orbitals. Due to their mirror symmetry the curvature of the tube does not break this symmetry, so that the tube remains strictly metallic. The Fermi level is $E_F = 0.0 \text{ eV}$ and k is in units of $[\pi/T_0]$.

$k_B T \approx 25 \text{ meV}$ ³¹ at the Fermi energy. A simple π -orbital tight-binding model,^{30,33,34} commonly employed in CNT transport simulations usually does not account for this effect, but such s-p hybridizations might be important to include when considering CNTs as possible candidates for interconnects. For tubes with diameters $d \leq 1 \text{ nm}$, the structural deformation of the graphene sheet affects its electronic structure significantly enough that such an opening of a bandgap can be induced. The opening arises due to a reduction of the overlap between the nearest-neighbor π -orbitals under deformation causing the Fermi wavevector k_F to move away from the K-point within the 1st Brillouin zone.^{31,35}

The more complex sp^3 - and the sp^3d^5 -EHT models we are using naturally account for these structural deformations (Figs. 4 and 5) through the structure-dependent overlap matrix \mathbf{S} , cf. Eq.(5), yielding for our bulk graphene parameters a gap that actually compares quite well quantitatively in the case of a sp^3 -model with experimental scanning tunneling spectra (cf. Table II), whereas our sp^3d^5 -model shows a poorer quantitative match for these class of tubes.

C. Ultrasmall Diameter Tubes

For ultrasmall nanotube diameters, hybridization effects start to become dominant. Fig. 6 shows that the (5,0) zig-zag tube, semi-conducting in a zone-folding method, is predicted by EHT to become metallic for the case of a sp-orbital model, since the valence and conduction bands cross at $E_F \approx 0.0 \text{ eV}$. On the other hand, the zig-zag (6,0) tube moves the other way (Fig. 7), from being metallic in a zone-folding method to semi-

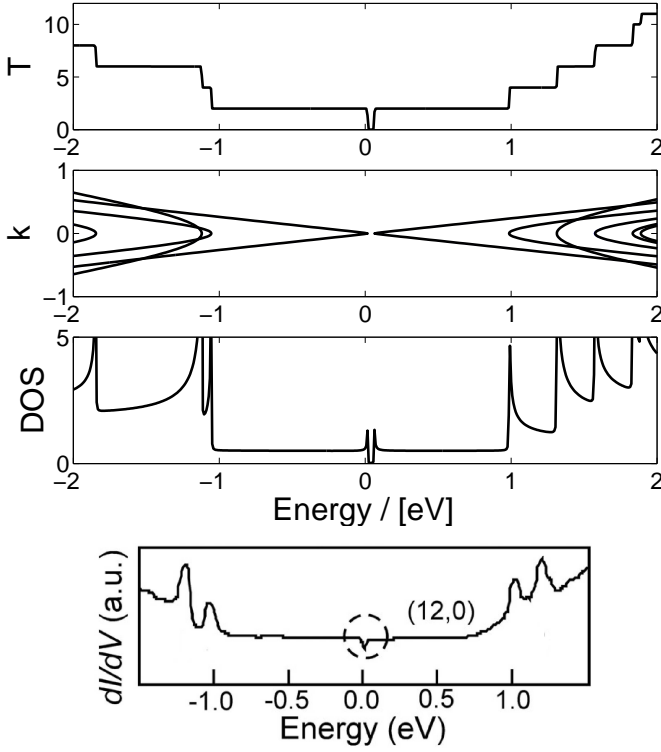


FIG. 4: Bandstructure, DOS, and transmission per spin for a “metallic” zig-zag (12,0) tube using sp^3 -orbitals. The gap close to the Fermi level at $E_F = 0.0$ eV is about 50 meV. For comparison the experimental STS- dI/dV signal is shown at the bottom³¹. The bottom figure has been “Reprinted (abstracted/excerpted) with permission from M. Ouyang, J.L. Huang, C.L. Cheung, and C.M. Lieber, “Energy Gaps in Metallic Single-Walled Carbon Nanotubes,” *Science*, **292**, 702 (2001). Copyright 2001 AASS.”

conducting in EHT with a bandgap of ≈ 0.12 eV due to strong hybridization effects. DFT-GGA calculations, however, show that a (6,0)-tube remains metallic due to re-hybridization.^{36,37} Using in turn spd-orbitals for carbon, our EHT-model agrees with the DFT-GGA results for these small diameter tubes. While the accuracy of DFT for semiconducting bandgaps is itself open to question, the contradictory result for the sp -orbital model could also imply that the inclusion of deformation effects through just the off-diagonal EHT Hamiltonian elements is no longer a valid assumption, and the onsite energies themselves need to be recalculated self-consistently to include the effect of the electrostatics on the local atomic potentials.

For large deformations a fully self-consistent calculation of the bandstructure might be necessary to describe the electronic structure properly. If the tube has a large curvature, the respective charge distributions inside and outside the tube become asymmetric³⁶ leading to the formation of dipoles. Due to the charge re-distribution and the dipolar electric fields the individual bands are shifted such that the (6,0) tube remains metallic in DFT-GGA. The processes of charge-redistribution, dipole-formation,

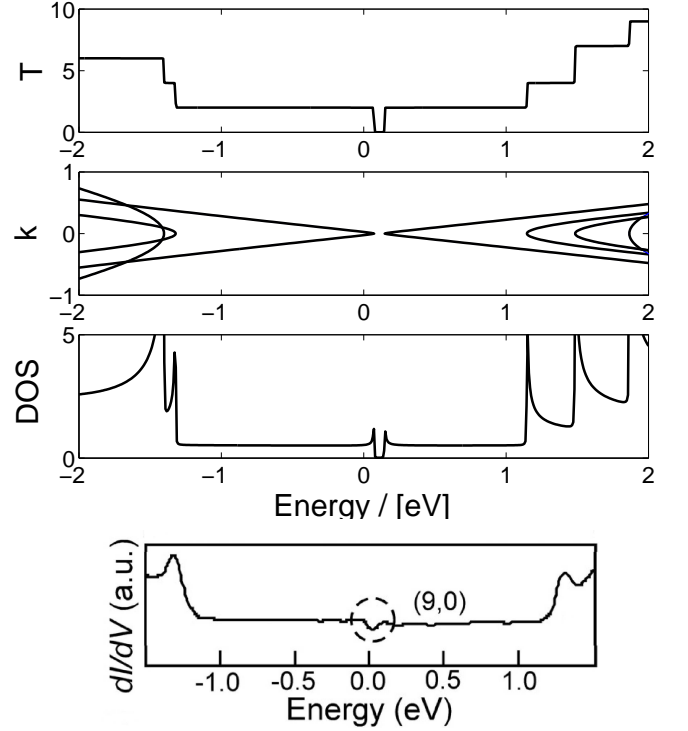


FIG. 5: Bandstructure, DOS, and transmission per spin for a “metallic” zig-zag (9,0) tube using sp^3 -orbitals. The gap close to the Fermi level at $E_F = 0.0$ eV is about 80 meV similar to STS- dI/dV measurements as shown at the bottom³¹. The bottom figure has been “Reprinted (abstracted/excerpted) with permission from M. Ouyang, J.L. Huang, C.L. Cheung, and C.M. Lieber, “Energy Gaps in Metallic Single-Walled Carbon Nanotubes,” *Science*, **292**, 702 (2001). Copyright 2001 AASS.”

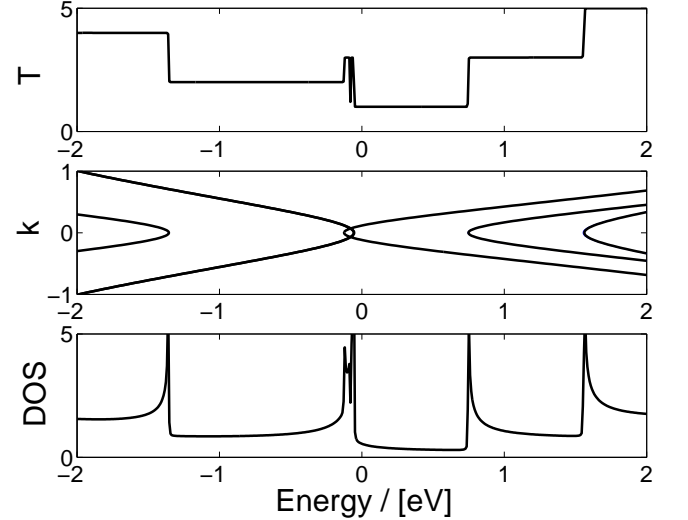


FIG. 6: Bandstructure, DOS, and transmission per spin for a zig-zag (5,0) tube using sp^3 -orbitals. Due to the crossing of the bands around $E_F \approx 0.0$ eV the tube becomes metallic.

(n, m)	TB	CNT-bands	DFT	Experiments	EHT-sp	EHT-spd
(5, 0)	—	1.91 ($\gamma = 2.5$) 2.29 ($\gamma = 3.0$)	0.0 ³⁷	—	-0.05	0.0
(6, 0)	0.05 ³⁶ ≈ 0.2 ⁴³ 0.179 ⁴⁵	0.0	-0.83 ³⁶ 0.0 ³⁷	—	0.12	0.0
(9, 0)	0.2 ³⁷ 0.075 ⁴⁵ 0.07 ³⁶ ≈ 0.04 ⁴³	0.0	0.2 (GGA) ³⁷ 0.17 (LDA) ³⁶ 0.12 (LDA) ³⁸ 0.17 (GW) ³⁸	0.080 ± 0.005 ³¹	0.075	0.13
(10, 0)	0.65 ⁴⁴ 0.87 ⁴⁴ 0.85 ⁴³	0.91 ($\gamma = 2.5$) 1.09 ($\gamma = 3.0$)	0.88 (GGA) ³⁷ 0.8 (GGA) ⁴⁶	0.83 ³²	0.91	0.95
(12, 0)	0.08 ³⁷ 0.0 ⁴³	0.0	0.08 (GGA) ³⁷ 0.057 (LDA) ³⁹	0.042 ± 0.004 ³¹	0.045	0.077
(13, 0)	≈ 0.7 ⁴³	0.70 ($\gamma = 2.5$) 0.84 ($\gamma = 3.0$)	0.73 (GGA) ³⁷	—	0.71	0.74
(15, 0)	0.0 ⁴³	0.0	0.14 (GGA) ³⁷ 0.038 (LDA) ³⁹	0.029 ± 0.004 ³¹	0.026	0.05
(16, 0)	—	0.56 ($\gamma = 2.5$) 0.68 ($\gamma = 3.0$)	0.61 (GGA) ³⁷	0.65 ± 0.30 ⁴⁰	0.59	0.6

TABLE II: Comparison of experimentally and theoretically determined bandgaps (in units [eV]) using different theoretical methods: TB denotes orthogonal tight-binding, CNT-bands refers to a simple π -orbital description with one hopping parameter γ , DFT is density-functional theory using different approximations for exchange-correlation potential, and EHT with sp- or spd-orbitals for carbon.²²

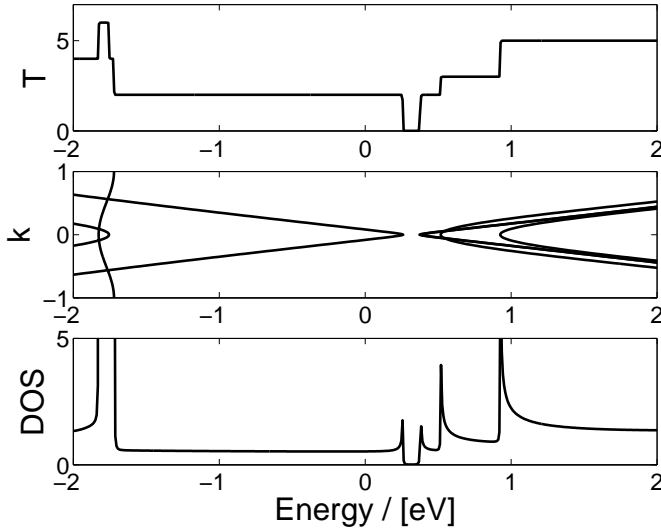


FIG. 7: Bandstructure, DOS, and transmission per spin for a zig-zag (6,0) tube using sp^3 -orbitals. The “metallic” tube becomes semi-conducting with a bandgap of ≈ 0.1 eV, and shift of the Fermi-level from 0.0 eV to ≈ 0.3 eV.

and the floating of the bands, however, require a fully self-consistent bandstructure calculation that can be set up within the Poisson NEGF approach,¹⁶ but has not yet been incorporated within our present computational scheme. Note, that this is not a shortcoming of the Extended Hückel Theory itself, but arises instead from the importance of self-consistent electrostatic effects that have been discarded for simplicity in the bandstructure calculation. Table II compares the bandgaps for the

studied tubes both with respect to STS experiments as well as other theoretical calculations. Our results based on Extended-Hückel Theory are in good agreement with more sophisticated DFT approaches and experiments – in fact, local density approximation (LDA) suffers from the well-known bandgap problem that an EHT approach calibrated to graphene seems to bypass. This suggests that an EHT scheme, supplemented by self-consistent electrostatics, might be a good compromise between simple π -orbital tight-binding theories and computationally expensive DFT-methods, the practicality of the scheme being particularly important when modeling transport through large complex nanostructures.

V. NANOTUBES AS CHEMICAL SENSORS

While the previous examples test our EHT prescription for bandstructure calculations of bare CNTs, we now combine it with molecule chemistry. It has been suggested that the chemisorption of CO molecules could be enhanced by deforming the CNT, so that the regions of highest curvature have an enhanced chemical reactivity.⁵¹ Based on a first principles calculation within GGA, da Silva *et al.* have shown that a semiconducting (8, 0) CNT can become metallic upon lateral deformation to an elliptical shape, but thereafter the semi-conducting state can be recovered by attaching a CO molecule at the spot of highest curvature.²⁴ This seems to indicate that highly deformed CNTs are possible candidates for sensing CO molecules by means of a bandgap variation and cor-

responding metal-insulator transition. We use the DFT calculations by da Silva *et al.* as a qualitative benchmark to explore the accuracy of EHT for electronic structure in the presence of a periodic array of CO molecules, of which one unit cell is shown in Fig. 8.

Our starting point is the bandstructure of an undeformed semiconducting (8,0) tube using spd-EHT parameters optimized for 2D-graphene with the Fermi-level set at $E_F = -13$ eV.²² The transferability of the sp- as well as the spd-orbital EHT-parameters have been discussed in the previous section. Setting our vacuum level as the zero energy reference, we shift the CNT Fermi energy by $V_c = +8.5$ eV towards the experimental Fermi-level of 2D-graphene, i.e. $E_F = -4.5$ eV, employing the modified Hückel prescription, cf. Eq. (6). Following Ref.²⁴ we deform the tube perpendicular to its axis so that the minor axis is 30% of the original tube radius of $R_t = 6.3$ Å, cf. Fig. 8.

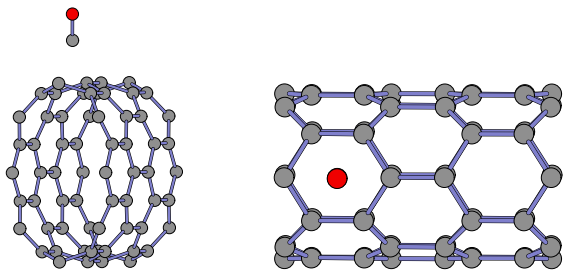


FIG. 8: Unit cell of a semi-conducting (8,0) CNT with one CO molecule at distance of $d = 1.85$ Å from the CNT surface. The CO molecule has been placed above the center of the hexagon which is the most stable equilibrium position after relaxation²⁴. The unit cell of the periodic structure consists of two (8,0) CNT unitcells and one CO molecule, i.e. the cell contains 66 atoms.

To ensure that our strongly deformed structure really corresponds to the local minimum of the total energy, we optimize the deformed tube unit cell by means of Gaussian 03⁴⁹ using the spin unrestricted LDA approach within the Vosko-Wilk and Nusair (SVWN) approximation. During the optimization we froze two rows atoms along the opposite extremes of the minor axis, while edge effects were eliminated from the optimized structure by employing periodic boundary conditions within Gaussian 03 for structure optimization, with a translation vector of 4.32 Å along the tube axis. We note that compared to da Silva *et al.*²⁴ our system being optimized consists of only one unit cell of a (8,0) tube instead of two.

Since the EHT levels are correct up to an overall shift, we start by aligning the levels of the CO molecule and the CNT. The highest occupied molecular orbital (HOMO) of CO, calculated within Gaussian 03 using the Becke 3 parameter exchange with Perdew-Wang 91 correlation (B3PW91) with 6-31g(d) basis sets is $E_H = -10.14$ eV relative to vacuum. The corresponding value in our EHT parametrization is $E_H = -14.09$ eV, so that we need an overall shift $V_{c,CO} = +3.95$ eV. After this shift is ex-

ecuted, the CO molecule is attached to the tube at the point where its curvature is highest. According to Ref.²⁴ the most favorable location to place the CO molecule is above the center of a hexagon, as shown in Fig. 8. Since we are only interested in the effect of one single CO molecule on the tube dispersion, we need to avoid any overlap between neighboring CO molecules. This is accomplished by using two CNT (8,0) unit cells and attaching only one CO molecule. The effective periodicity of the system is then 8.64 Å, large enough that the neighboring CO molecular basis functions do not overlap.

Figure 9 shows the dispersion, and Fig. 10 the respective DOS and transmission per spin for the combined CNT-molecular system. The original bandgap $E_G = 1.1$ eV of the undeformed tube (left) shrinks down to $E_G \approx 30$ meV upon the 30% lateral deformation, so that the tube becomes effectively metallic at room temperature (center). Attachment of the CO molecule on the deformed CNT (right) makes the tube semiconducting once again, with a bandgap of $E_G \approx 100$ meV, much less than that of the undeformed tube, but noticeably larger than thermal energies at room temperature. Our results agree qualitatively with da Silva *et al.*,^{24,51} even though there are quantitative differences: the initial bandgap of the undeformed tube is 0.66 eV and becomes completely closed after lateral deformation, so that the tube becomes truly metallic. The recovered bandgap upon CO-attachment is with ≈ 200 meV, of similar order as in our case with 100 meV. The largest source of disagreement is the bandgap of the undeformed CNT; given that DFT bandgaps (see Table II) are often questionable as well, a quantitative resolution of this discrepancy may need experimental attention.

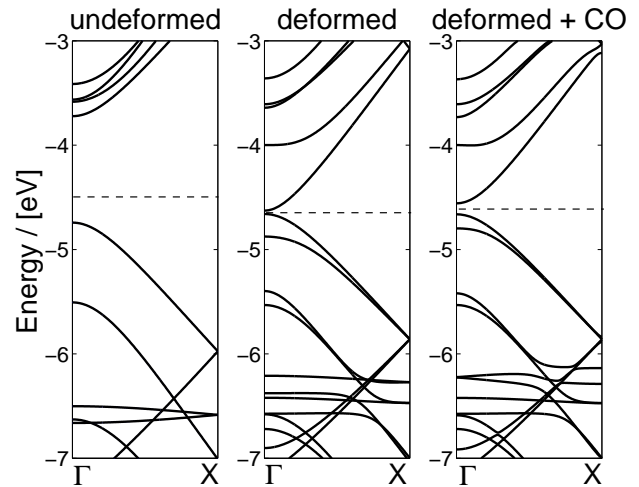


FIG. 9: Bandstructures of a zig-zag (8,0) CNT using sp^3d^5 -orbitals. Left: undeformed tube with a bandgap of $E_G \approx 1.1$ eV, middle: deformed tube with a small gap of $E_G \approx 25$ meV, and right: deformed tube with attached CO molecule at distance 1.85 Å. The gap here is $E_G \approx 100$ meV. The Fermi energy is indicated by the dashed line.

Note that the present calculations are all non-self-

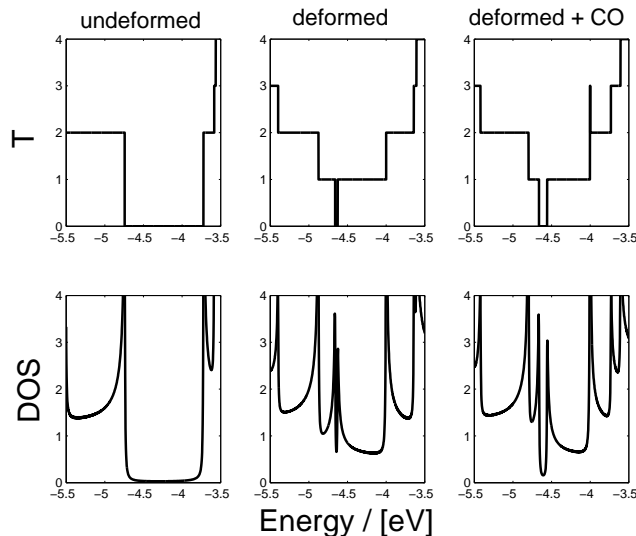


FIG. 10: DOS and transmission per spin for the semi-conducting (8,0) CNT: left: undeformed, middle: deformed, and right: deformed with attached CO-molecule.

consistent, ignoring effects due to the rearrangement of charges during tube deformation, as well as those arising from charge transfer between the molecular species and the nanotube, while a proper self-consistent calculation as discussed in the last section, is needed to do quantitative justice to this problem. Nonetheless, the EHT parameters seem to be quite transferable between bandstructure as well as surface chemistry, in particular for strongly deformed structures without the need for any reparametrization. This makes EHT a good compromise between accuracy and practicality. In our follow-up paper, we will demonstrate the applicability of EHT to modeling silicon, including its transferability between bulk and multiple surface bandstructures of reconstructed silicon surfaces and also for nanowires. Applying this approach has allowed us to quantitatively explain and in some cases even predict interesting experimental results involving molecular conductors on silicon.^{1,2}

VI. FUTURE WORK

For transport calculations, we often need a minimal model that can do justice to bandstructure, electrostatic

as well as bonding chemistry. This becomes particularly important if one wants to deal with strongly deformed structures, interfaces or combinations thereof including molecules. We have shown that Extended Hückel Theory provides a good practical compromise to capture various aspects of bandstructure and chemistry. The two attributes that make this semi-empirical approach especially useful are the presence of explicit basis-sets and non-orthogonality. To make this chemists' approach to bandstructure of further use, it may be preferable to work with a self-consistent *complete neglect of differential overlap* (CNDO) approach to bring in differential Coulomb costs into the picture.

For many nanoscale structures such as nanotubes and nanowires perhaps even interfacing with smaller molecules, we believe that a semi-empirical approach combining bandstructure and chemistry is essential, given that typical tight-binding theories are not transferable beyond small deformations while DFT theories are computationally quite prohibitive. The latter becomes even more difficult to implement when we want to move from equilibrium electronic structure to more complicated nonequilibrium transport problems. It is generally acknowledged that much of the conducting properties of nanostructures are dominated by their interfaces and contacts. It is in this complicated domain that we believe the real strength of a non-orthogonal theory with explicit basis sets such as EHT or CNDO is likely to manifest itself.

Acknowledgement

We acknowledge the support of the Army Research Office through the Defense University Research Initiative in Nanotechnology (DURINT) program, and the Army Research Office. J. Cerda acknowledges support from the Spanish DGICYT and CAM under contract No. MAT2004-05348-C04-2 and MAT/0440/2004, respectively. The authors are indebted to M.P. Anantram for his help and discussions. We thank K.H. Bevan, H. Raza, L. Siddiqui, and M.S. Lundstrom for helpful discussions.

* Electronic address: kienle@ecn.purdue.edu

¹ T. Rakshit, G.C. Liang, A.W. Ghosh, and S. Datta, "Silicon-based Molecular Electronics" *Nano.Lett.*, **4** 1803 (2004).

² G.C. Liang and A.W. Ghosh, "Identifying Contact Effects in Electronic Conduction through C_{60} on Silicon," *Phys.Rev.Lett.*, **95**, 076403 (2005).

³ J. Park, A.N. Pasupathy, J.I. Goldsmith, C. Chang, Y.

Yaish, J.R. Petta, M. Rinkoski, J.P. Sethna, H.D. Abruna, P.L. McEuen, and D.C. Ralph, "Coulomb blockade and the Kondo effect in single-atom transistors," *Nature*, **417**, 722 (2002).

⁴ B. Muralidharan, A.W. Ghosh, and S. Datta, "Probing electronic excitations in molecular conduction," *cond-mat/0505375 v2* 25 Oct 2005.

⁵ C. M. Goringe, D.R. Bowler, and E. Hernandez, "Tight-

- Binding Modelling of Materials” *Rep.Prog.Phys.*, **60**, 1447 (1997).
- ⁶ A. Peccia and Aldo Di Carlo, “Atomistic Theory of Transport in Organic and Inorganic Nanostructures” *Rep.Prog.Phys.*, **67**, 1497 (2004).
 - ⁷ D. Kienle and A.W. Ghosh, “Atomistic Modeling of Metal-Nanotube Contacts” *J.Comp.El.*, **4**, 97 (2005).
 - ⁸ P. Vogl, H.P. Hjalmarson, and J.D. Dow, “A Semi-Empirical Tight-Binding Theory of the Electronic Structure of Semiconductors” *J.Phys.Chem. Solids*, **44**, 365 (1983).
 - ⁹ J.-M. Jancu, R. Scholz, F. Beltram, and F. Bassani, “Empirical sp^3s^* tight-binding calculation for cubic semiconductors: General method and material parameters” *Phys.Rev.B*, **57**, 6493 (1998).
 - ¹⁰ T. Boykin, G. Klimeck, and F. Oyafuso, “Valence band effective mass expressions in the $sp^3d^5s^*$ empirical tight-binding model applied to a Si and Ge parametrization” *Phys.Rev.B*, **69**, 115201 (2004).
 - ¹¹ P. N. Keating, “Effect of Invariance Requirements on the Elastic Strain Energy of Crystals with Application to the Diamond Structure,” *Phys.Rev.*, **145**, 637 (1966).
 - ¹² R.G. Parr and W. Yang, *Density-Functional Theory of Atoms and Molecules* New York: Cambridge University Press, 1994.
 - ¹³ U. von Barth, “Basic Density Functional Theory - an Overview,” *Physica Scripta*, **T109**, 9 (2004).
 - ¹⁴ R.M. Martin, *Electronic Structure: Basic Theory and Practical Methods* New York: Cambridge University Press, 1994.
 - ¹⁵ J. Taylor, H. Guo, and J. Wang, “Ab initio modeling of quantum transport properties of molecular electronic devices” *Phys.Rev.B*, **63**, 245407 (2001).
 - ¹⁶ P. S. Damle, A. W. Ghosh, and S. Datta, “Unified description of molecular conduction: From molecules to metallic wires,” *Phys.Rev.B*, **64**, 201403 (2001).
 - ¹⁷ M. Brandbyge, J.-L. Mozos, P. Ordejón, J. Taylor, and K. Stokbro, “Density-functional method for nonequilibrium electron transport,” *Phys.Rev.B*, **65**, 165401 (2002).
 - ¹⁸ N. Sai, M. Zwolak, G. Vignale, and M. Di Ventra, “Dynamical corrections to the DFT-LDA electron conductance in nanoscale systems,” cond-mat/0411098 v2 21 Feb 2005
 - ¹⁹ J. N. Murrell and A. J. Harget, *Semi-empirical self-consistent-field molecular orbital theory of molecules* New York: Wiley-Interscience, 1972.
 - ²⁰ W. Tian, S. Datta, S. Hong, R. Reifenberger, J. Henderson and C.P. Kubiak, “Conductance Spectra of Molecular Wires”, *J. Chem. Phys.* **109**, 2874-2882 (1998).
 - ²¹ J. Cerdà and F. Soria, “Accurate and transferable extended Hückel-type tight-binding parameters,” *Phys.Rev.B*, **61**(12), 7965 (2000).
 - ²² <http://www.icmm.csic.es/jcerda/index.html>.
 - ²³ J.M. Soler, E. Artacho, J.D. Gale, A. Garcia, J. Junquera, P. Ordejón, and D. Sanchez-Portal “The Siesta method for ab initio order-N materials simulation,” *J. Phys.: Cond. Mat.* **14**, 2745 (2002).
 - ²⁴ L.B. da Silva, S.B. Fagan, and R. Mota, “Ab Initio Study of Deformed Carbon Nanotube Sensors for Carbon Monoxide Molecules,” *Nano.Lett.*, **4**, 65 (2004).
 - ²⁵ H. Haug and A. P. Jauho, *Quantum Kinetics in Transport and Optics of Semiconductors*, Berlin: Springer, 1996.
 - ²⁶ S. Datta, *Electronic Transport In Mesoscopic Systems*, New York: Cambridge University Press, 1995.
 - ²⁷ M.P.L. Sancho, J.M.L. Sancho, and J. Rubio, “Quick iterative scheme for the calculation of transfer matrices: application to Mo (100),” *J.Phys.F: Met.Phys.*, **14**, 1205 (1984).
 - ²⁸ M.P.L. Sancho, J.M.L. Sancho, and J. Rubio, “Highly convergent schemes for the calculation of bulk and surface Green functions,” *J.Phys.F: Met.Phys.*, **15**, 851 (1985).
 - ²⁹ J. C. Slater and G. F. Koster, “Simplified LCAO Method for the Periodic Potential Problem,” *Phys.Rev.*, **94**, 1498 (1954).
 - ³⁰ R. Saito, G. Dresselhaus, and M.S. Dresselhaus, *Physical Properties of Carbon Nanotubes* London: Imperial College Press, 2003.
 - ³¹ T.W. Odom, M. Ouyang, J.L. Huang, C.L. Cheung, and C.M. Lieber, “Energy Gaps in Metallic Single-Walled Carbon Nanotubes,” *Science*, **292**, 702 (2001).
 - ³² T.W. Odom, J.L. Huang, P. Kim, and C.M. Lieber, “Structure and Electronic Properties of Carbon Nanotubes,” *J.Phys.Chem.B*, **104**, 2794 (2000).
- Note: Since the value for the (8,0) CNT is not given explicitly, we have determined its bandgap from the STS-plot by measuring the distance between the 1st VHS where the STS is negligible, so that a gap can be clearly identified. The distance between the largely broadened peaks is about 1.1 eV.
- ³³ F. Triozon, P. Lambin, and S. Roche, “Electronic transport properties of carbon nanotube based metal/semiconductor/ metal intramolecular junctions,” *Nanotechnology*, **16**, 230 (2005).
 - ³⁴ H. Liu and Y. Tao, “Coherent transport between two interface states in single-walled carbon nanotube quantum dots,” *Nanotechnology*, **16**, 619 (2005).
 - ³⁵ L. Yang and J. Han, “Electronic Structure of Deformed Carbon Nanotubes,” *Phys.Rev.Lett.*, **85**, 154 (2000).
 - ³⁶ X. Blase, L.X. Benedict, E.L. Shirley, and S.G. Louie, “Hybridization Effects and Metallicity in Small Radius Carbon Nanotubes,” *Phys.Rev.Lett.*, **72** (12), 1878 (1994).
 - ³⁷ G. Sun, J. Kürti, M. Kertesz, and R.H. Baughman, “Variations of the Geometries and BandGaps of Single-Walled Carbon Nanotubes and the Effect of Charge Injection,” *J.Phys.Chem. B*, **107**, 6924 (2003).
 - ³⁸ T. Miyake and S. Saito, “Bandgap-formation in (n,0) single-walled carbon-nanotubes (n = 9,12,15,18): A first principles study,” *Phys.Rev.Lett.*, **72**, 073404 (2005).
 - ³⁹ T. Miyake: The bandgaps for the (12,0) and (15,0) CNT are based on LDA-calculations (private communication).
 - ⁴⁰ J.W.G. Wildboer, L.C. Venema, A.G. Rinzler, R.E. Smalley, and C. Dekker, “Electronic structure of atomically resolved carbon nanotubes,” *Nature*, **391**, 59 (1998).
 - ⁴¹ L.C. Venema, V. Meunier, Ph. Lambin, and C. Dekker, “Atomic structure of carbon nanotubes from scanning tunneling microscopy,” *Phys.Rev.B*, **61**, 2991 (2000).
 - ⁴² L.C. Qin, X. Zhao, K. Hirahara, Y. Miyamoto, Y. Ando, and S. Iijima, “The smallest carbon nanotube,” *Nature*, **408**, 50 (2000).
 - ⁴³ N. Hamada, S. Sawada, and A. Oshiyama, “New One-Dimensional Conductors: Graphitic Microtubules,” *Phys.Rev.Lett.*, **68**, 1579 (1992).
 - ⁴⁴ H. Yorikawa and S. Muramatsu, “Energy Gaps of semiconducting nanotubules,” *Phys.Rev.B*, **52**, 2723 (1995).
 - ⁴⁵ J.X. Cao, X.H. Jan, J.W. Ding, and D.L. Wang, “Band structures of carbon nanotubes: the sp^3s^* tight-binding model,” *J.Phys.C*, **13**, L271 (2001).
 - ⁴⁶ P.V. Avramov, K.N. Kudin, and G.E. Scuseria, “Single wall carbon nanotubes density of states: comparison experiment and theory,” *Chem.Phys.Lett.*, **370**, 597 (2003).

- ⁴⁷ S. Reich, J. Maultzsch, and C. Thomsen, “Tight-binding description of graphene,” *Phys.Rev.B*, **66**, 035412 (2002).
- ⁴⁸ C. J. Park *et al.*, “Band-gap modification by radial deformation in carbon nanotubes,” *Phys.Rev.B*, **60**, 10656 (1999).
- ⁴⁹ Gaussian 03, Revision C.02, M. J. Frisch, G. W. Trucks, H. B. Schlegel, G. E. Scuseria, M. A. Robb, J. R. Cheeseman, J. A. Montgomery, Jr., T. Vreven, K. N. Kudin, J. C. Burant, J. M. Millam, S. S. Iyengar, J. Tomasi, V. Barone, B. Mennucci, M. Cossi, G. Scalmani, N. Rega, G. A. Petersson, H. Nakatsuji, M. Hada, M. Ehara, K. Toyota, R. Fukuda, J. Hasegawa, M. Ishida, T. Nakajima, Y. Honda, O. Kitao, H. Nakai, M. Klene, X. Li, J. E. Knox, H. P. Hratchian, J. B. Cross, V. Bakken, C. Adamo, J. Jaramillo, R. Gomperts, R. E. Stratmann, O. Yazyev, A. J. Austin, R. Cammi, C. Pomelli, J. W. Ochterski, P. Y. Ayala, K. Morokuma, G. A. Voth, P. Salvador, J. J. Dannenberg, V. G. Zakrzewski, S. Dapprich, A. D. Daniels, M. C. Strain, O. Farkas, D. K. Malick, A. D. Rabuck, K. Raghavachari, J. B. Foresman, J. V. Ortiz, Q. Cui, A. G. Baboul, S. Clifford, J. Cioslowski, B. B. Stefanov, G. Liu, A. Liashenko, P. Piskorz, I. Komaromi, R. L. Martin, D. J. Fox, T. Keith, M. A. Al-Laham, C. Y. Peng, A. Nanayakkara, M. Challacombe, P. M. W. Gill, B. Johnson, W. Chen, M. W. Wong, C. Gonzalez, and J. A. Pople, Gaussian, Inc., Wallingford CT, 2004.
- ⁵⁰ D. Papaconstantopoulos, *Handbook of the Bandstructure of Elemental Solids*, New York: Plenum Press, 1986.
- ⁵¹ S.B. Fagan, L.B. da Silva, and R. Mota, “Ab initio Study of Radial Deformation Plus Vacancy on Carbon Nanotubes: Energetics and Electronic Properties,” *Nano.Lett.*, **3**, 289 (2003).
- ⁵² Note, that in the EHT-parameter optimization the Fermi level for graphene is set to $E_F = -13$ eV, so that the bands are unique up to an overall shift.^{21,22} The role of the Fermi energy in parameter fitting has been addressed in section III. Its absolute value, however, becomes particularly important for compound systems as shown in section V.